Self-Assembly of Small Polycyclic Aromatic Hydrocarbons on Graphite: A Combined Scanning Tunneling Microscopy and Theoretical Approach

Gina M. Florio, Tova L. Werblowsky, Thomas Müller,† Bruce J. Berne,* and George W. Flynn*

Department of Chemistry, The Environmental Molecular Sciences Institute, and The Center for Electron Transport in Molecular Nanostructures, Columbia University, New York, New York 10027

Received: August 6, 2004; In Final Form: December 29, 2004

Self-assembled monolayers of chrysene and indene on graphite have been observed and characterized individually with scanning tunneling microscopy (STM) at 80 K under low-temperature, ultrahigh vacuum conditions. These molecules are small, polycyclic aromatic hydrocarbons (PAHs) containing no alkyl chains or functional groups that are known to promote two-dimensional self-assembly. Energy minimization and molecular dynamics simulations performed for small groups of the molecules physisorbed on graphite provide insight into the monolayer structure and forces that drive the self-assembly. The adsorption energy for a single chrysene molecule on a model graphite substrate is calculated to be 32 kcal/mol, while that for indene is 17 kcal/mol. Two distinct monolayer structures have been observed for chrysene, corresponding to high- and low-density assemblies. High-resolution STM images taken of chrysene with different bias polarities reveal distinct nodal structure that is characteristic of the molecular electronic state(s) mediating the tunneling process. Density functional theory calculations are utilized in the assignment of the observed electronic states and possible tunneling mechanism. These results are discussed within the context of PAH and soot particle formation, because both chrysene and indene are known reaction products from the combustion of small hydrocarbons. They are also of fundamental interest in the fields of nanotechnology and molecular electronics.

Introduction

With its ability to provide spatial information at the atomic scale, scanning tunneling microscopy (STM) has become one of the most important experimental techniques in the fields of chemistry and physics as well as molecular electronics and nanotechnology. STM provides detailed information about the spatial and electronic properties of both surfaces and molecular assemblies. The technique has been used to interrogate molecular self-assembly under a variety of conditions,[1−10] to build and characterize nanoscale devices,[11,12] to follow dynamics and chemical reactions on surfaces,[12−21] and even to initiate chemical reactions.[12] The versatility of STM is limited only by its inability to distinguish different chemical groups or atoms; however related techniques such as scanning tunneling spectroscopy and inelastic electron tunneling spectroscopy can in principle provide unique electronic or vibrational signatures for surface atoms and adsorbate functional groups.[12,22−30]

Numerous STM studies have focused on understanding the spontaneous self-assembly of molecules on surfaces, including the physisorbed monolayers formed at the liquid−graphite interface[1,3−5,8−10,18,21,28,31−41] and the vacuum−graphite interface.[23−25,42−52] Information about the factors that promote two-dimensional self-assembly, such as van der Waals forces, electrostatic forces, and hydrogen-bonded interactions, has been gleaned from these investigations. Although these types of forces, their relative strengths, and their importance for self-assembly are properties that cannot be easily measured by experiments, complementary theoretical studies can provide quantitative information about contributions by individual types of interactions. When combined with experimental data, the theoretical results provide a more complete understanding of the forces that drive two-dimensional self-assembly.

Progress in the bottom-up fabrication of molecular electronic devices will depend on our ability to exploit the two-dimensional self-organization of molecules at interfaces. To control self-assembly, it is important to first understand the forces that drive the spontaneous ordering of molecules at interfaces. Once a fundamental understanding of these forces has been obtained, the engineering of specific structures should become routine. The ability to control self-assembly and create well-defined structures suggests the possibility of utilizing surface templates to investigate and control chemical reactivity on these surfaces.

Because of the interest in using large π-conjugated molecules as organic semiconductors, numerous STM studies have been carried out to characterize such molecules on surfaces under a variety of conditions.[2,6,22−24,26,28,29,34−38,42,43,53−56] These molecules have attracted attention in the context of charge transport as materials for molecular electronic device applications. Aromatic molecules, whose conductivity occurs via the π-system, can behave as either electron donors or acceptors, depending on their functionalization. Also, because the electronic band gap scales inversely with size, such π-conjugated molecules offer a degree of flexibility in the design of electronic devices. The size of the aromatic π-system and the substitution of electron-accepting or -donating groups allow for well-defined, specific tuning of the hole/electron transport properties.

The goal of the present work is to characterize the geometric arrangements and electronic properties of small polycyclic

* Authors to whom correspondence should be addressed: Phone (212) 854-2186 (B.B.); (212) 854-4162 (G.F.). E-mail: berne@chem.columbia.edu; flynn@chem.columbia.edu.

† Current Address: Veeco Metrology Group, 112 Robin Hill Road, Santa Barbara, CA 93117.

10.1021/jp046458v CCC: $30.25 © 2005 American Chemical Society
Published on Web 02/18/2005

aromatic hydrocarbons (PAHs) on graphite surfaces using a combined STM and theoretical approach. An additional goal is to address the potential use of such systems to investigate surface chemical reactions leading to soot particle growth and oxidation. Soot formation from the incomplete combustion of small hydrocarbons has been extensively studied in the gas phase, in flames, and with theoretical methods.[57,58] Far fewer studies have been focused on understanding soot particle nucleation and growth via surface reactions.[57,58] Environmental pollution and adverse health effects, arising from combustion byproducts such as PAHs and soot, drive interest in understanding the chemistry that transforms small hydrocarbons into PAHs and ultimately into particulate matter.

The present work illustrates the use of STM to identify and characterize the small PAH molecules chrysene and indene (see below) on graphite surfaces under low-temperature, ultrahigh

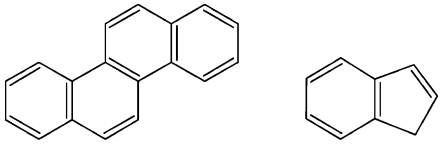

vacuum conditions. These molecules are known reaction products in sooting flames[57−63] and other combustion processes.[64,65] To a first approximation, soot particles can be thought of as small pieces of graphite that grow due to successive additions of acetylene to a radical species followed by cyclization.[57] Thus, bulk graphite serves as a model system on which to study soot particle surface chemistry. The reactions of such radical precursors, PAHs, and linear hydrocarbons with the surface of soot particles are themselves subjects of fundamental importance in combustion processes. Potentially, STM can be utilized to study the behavior of these species on graphite surfaces[66] to identify key chemical reactions that are important for the formation and growth of soot and to complement the wealth of gas-phase combustion chemistry experiments. Such studies can bridge the gap between important gas-phase combustion chemistry and surface-mediated reactions, leading to a more complete understanding of soot particle growth and oxidation mechanisms.

Methods

I. Experimental. Scanning tunneling microscopy (STM) experiments were conducted in an ultrahigh vacuum (UHV) chamber with a base pressure of 1×10^{-10} Torr. The UHV chamber is equipped with a quadrupole mass spectrometer (Stanford Research Systems RGA 200) and a variable temperature STM (Omicron Vakuumphysik GmbH) along with other surface analysis instrumentation. Highly oriented pyrolytic graphite (HOPG) (Advanced Ceramics, *zyb* grade) was freshly cleaved and immediately introduced into the vacuum system. The HOPG was cleaned by heating to 820 K for ∼20 min prior to deposition of molecular adsorbates.

For chrysene, the film was prepared by vacuum sublimation in a small extension chamber attached to the main UHV chamber. Vapor deposition was performed using an evaporator with a molybdenum crucible and a type-K thermocouple. Chrysene (98% pure) was obtained commercially (Aldrich) and degassed at 358−363 K for ∼12−24 h prior to each deposition. The chrysene sample was heated to 373 K for deposition onto the room-temperature HOPG substrate at a rate of 6−8 Å/min. The deposition rate was monitored with a quartz crystal microbalance (Sigma Instruments). The chrysene−HOPG sample was then transferred into the main UHV chamber and slowly annealed to 360 K. This gentle annealing process is intended to remove any multilayers of chrysene and give the remaining monolayer sufficient time and thermal energy to reach a minimum free energy structure. For STM measurements, the sample was cooled to 80 K using a liquid helium flow cryostat with the tip remaining near room temperature.

Indene possesses a high enough vapor pressure at room temperature to be deposited onto a cold HOPG substrate using a retractable line doser. Prior to deposition, indene (Aldrich, neat) was purified by at least 10 freeze−pump−thaw cycles. To ensure the presence of the compound in the gas phase without impurities, mass spectra were obtained prior to deposition and compared with the known spectrum.[67] Clean HOPG was transferred into the STM stage and slowly cooled to 190 K with the liquid helium cryostat prior to indene deposition. The line doser was positioned in the vicinity of the cold substrate, and ∼10 L of indene was vapor-deposited onto the graphite. Temperature programmed desorption data for *n*-decane on graphite[68,69] was used to estimate the multilayer desorption temperature for indene. The vapor pressure and mass of indene and *n*-decane are similar, suggesting that at a deposition temperature of 190 K the indene monolayer will be stable while multilayers will desorb. After a few minutes at the dosing temperature, the sample was further cooled to 80 K for analysis via STM.

STM tips were prepared by electrochemical AC etching of a polycrystalline tungsten wire. All images were taken in constant current mode. Typical scanning conditions are a +2 V bias between the tip and the surface, 100 pA tunneling current, and a scan rate of 6−8 lines/second. The effects of thermal and mechanical drift were minimized through use of the real-time drift correction available in the Omicron imaging software. Specific tunneling parameters are given for individual images in the figure captions, with the sign of the voltage referred to the sample.

II. Computational Modeling. Density functional theory (DFT) geometry optimization and frontier orbital calculations were performed for chrysene employing Becke's three-parameter exchange functional (Becke3),[70] Lee, Yang, and Parr's correlation functional (LYP),[71] and the lacvp basis set[72] within JAGUAR.[73] For simplicity of computation, the geometry optimization and frontier orbital calculations were performed on a single chrysene molecule in a vacuum. This is expected to be a fairly good approximation to the electronic structure of a chrysene monolayer because the molecules are weakly physisorbed on the graphite, and the only adsorbate−substrate interactions present are van der Waals forces.

To aid in understanding the spontaneous self-assembly of chrysene and indene on graphite, energy minimization and molecular dynamics simulations were performed for small clusters of molecules adsorbed on a model graphite surface using SIM,[74] a program written at Columbia University. Energy minimizations are performed on initial structures consistent with the STM images, both with and without periodic boundary conditions. The truncated Newton algorithm[75] is used to locate the minimum potential energy structure of each starting configuration. Constant NVT molecular dynamics (MD) simulations, thermally equilibrated with the Nose−Hoover chains method,[76] are then performed on the minimized structures under conditions approximating the experiments. The MD simulations determine the effect of thermal energy on the minimized packing assembly.

The HOPG substrate is modeled using the Steele potential.[77] The top two graphite layer sheets are described using a fully corrugated potential, and an additional 38 layers below the top two sheets are modeled as a smoothed-out, attractive potential. This simplification of the graphite structure has proven to be more than adequate in other theoretical studies of surface adsorption.[77−79]

The adsorbate intramolecular and intermolecular energetics are described using Jorgensen's OPLS-AA force field.[80] Intramolecular energy is described by harmonic bond stretches, bends, and torsions as well as by Lennard-Jones (6−12) dispersions, repulsions and electrostatic interactions between atoms separated by at least three bonds (1−4 interactions), both of which are scaled by 0.5 in this model. Intermolecular energy is described by electrostatic interactions (point charges) and Lennard-Jones (6−12) van der Waals dispersion and repulsion interactions. The strength of the adsorbate−substrate interaction is given by the Steele energy term. Image charges between the molecules and the substrate can also be added to the model; however, they have been neglected in the present analysis because they are quite small and when included they do not alter the optimized structures.

The data are presented as follows. The total potential energy is reported, along with a breakdown of its component contributions. The internal energy for the molecule or cluster of molecules on graphite is the sum of the stretch, bend, and torsional energies. Contributions to the total potential energy from van der Waals (Lennard-Jones) interactions, electrostatic interactions, and adsorbate−substrate (Steele) interactions are reported separately. The total potential energy of the system is thus the sum of the internal, electrostatic, Lennard-Jones, and Steele energies. All energies are reported in kcal/mol for the entire cluster. The total energy in each case is not scaled to a *per molecule* value because some simulations were performed without periodic boundary conditions. Without such boundary conditions, the edge molecules are not expected to have the same energy relative to the more internal molecules of the cluster, and thus reporting energies scaled for a single molecule would be deceptive. For example, a different configuration of molecules with the same relative orientations but with different numbers of edge versus internal molecules is expected to give a different value for the total energy of the system under study.

While the absolute, total potential energy for each system is given, it is sometimes helpful to compare cluster stabilization energies (or pair interaction energies for chrysene dimers on graphite) that are corrected for contributions from a single molecule adsorbed on the surface, which has a nonzero total potential energy of interaction. The stabilization energy (E_{stab}) for a cluster of N molecules on graphite is given by

$$E_{stab} = E_{cluster} - N(E_{monomer})$$

where $E_{cluster}$ is the absolute energy for the N molecule system and $E_{monomer}$ is the absolute energy for a single molecule of the cluster adsorbed on graphite in the absence of other molecules. While the absolute energies are influenced by the quality of the fit to the force field used in the calculation and therefore may suffer from the usual restrictions on absolute parameter accuracy for condensed-phase calculations, a comparison of relative energies is expected to provide a reliable measure of the stability of one possible structure over another.

Results

I. Chrysene: UHV−STM. Individual monolayers of chrysene are formed on the basal plane of graphite. Two distinct packing structures have been observed individually, a low-density monolayer (Figure 1a) and a high-density, close-packed monolayer (Figure 1b). Both structures exhibit well-ordered domains extending for several hundred nanometers, 20 nm by 20 nm portions of which are shown in Figure 1.

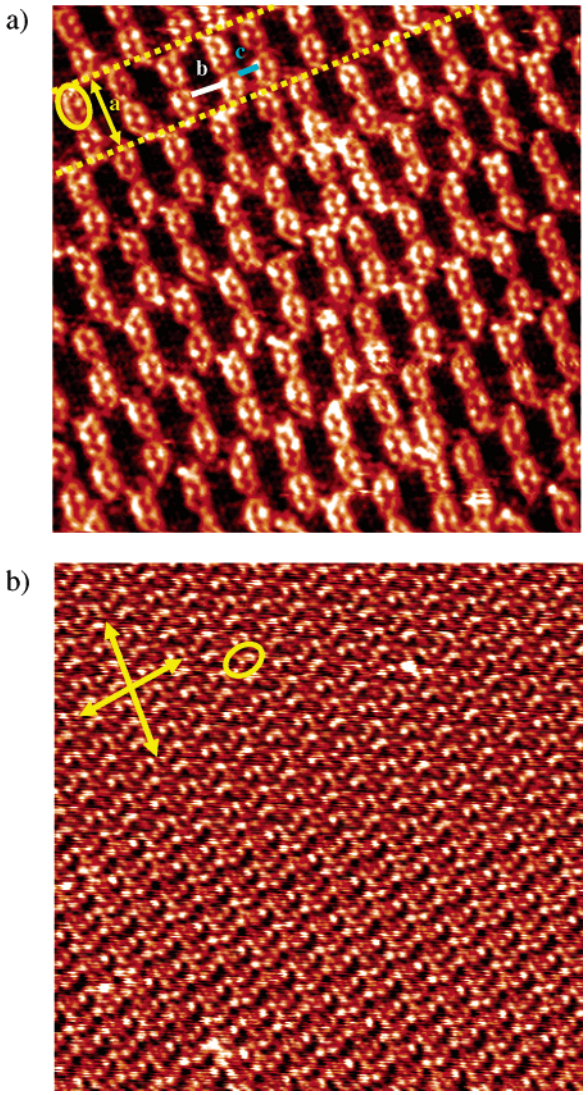

Figure 1. STM images of two distinct monolayer structures of chrysene on graphite under UHV conditions at 80 K. (a) A 20 nm by 20 nm STM topographic image of the low-density structure obtained at +1.85 V, 90 pA, 7 Hz, with active drift control. (b) A 20 nm by 20 nm STM topographic image of the high-density packing structure obtained at +1.90 V, 100 pA, 7 Hz, with active drift control. In the low-density structure (a), a single chrysene molecule is shown within the yellow oval, the chrysene molecules pack as dimers (a = 2.2 nm) with large amounts of empty space between the pairs, and the rows of dimers (b = 0.5 nm), indicated by yellow dashed lines, are offset from adjacent rows. Packing defects are observed in part a as changes in the spacing between molecules (c vs b), and the underlying HOPG spot pattern is observed in the spaces between molecules. In part b, the yellow arrows indicate the lamellar directions, and the oval indicates the size of a single chrysene molecule.

In the low-density configuration, the chrysene molecules assemble as rows of dimers with a large amount of space between each pair, as indicated by the dotted yellow lines in the STM image (Figure 1a). A single chrysene molecule is observed within the yellow oval. Adjacent rows of molecules are offset from one another and form large, empty cavities between the dimer pairs. The length of the cavity, a, is about 2.2 nm and is shown by the yellow arrow in the STM image

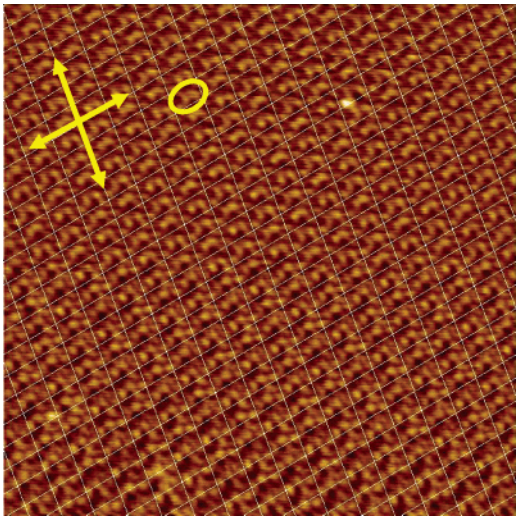

Figure 2. The Fourier transform autocorrelation of the STM topograph shown in Figure 1a. The unit cell grid is overlaid on the image. The unit cell parameters ($a = 0.80$ nm, $b = 1.23$ nm, $\alpha = 80°$) are consistent with the size of a single chrysene molecule. The lamellar axes are indicated by the yellow arrows, and a single molecule is identified by the yellow oval.

(Figure 1a). At least three rows of bare graphite are visible between the dimer pairs, corresponding to a neighbor spacing, *b*, of about 0.5 nm. Upon close inspection (Figure 1a), the hexagonal tunneling signature of graphite can be observed along a given lamella. No strong Moiré effect is observed, suggesting that each molecule occupies an equivalent adsorption site and a commensurate superstructure is formed by the molecules on the graphite substrate. The low-density monolayer contains numerous defects such as empty holes (not shown) or places where the spacing between molecules changes (Figure 1a). One such location where a significantly smaller neighbor spacing, *c*, is observed is indicated by the blue bar in the STM image (Figure 1a).

Direct observation of the tunneling signature of graphite suggests that only a monolayer of chrysene is present in the low-density configuration. It is highly unlikely that a second layer of chrysene molecules are lying directly above the monolayer, leaving large empty cavities on the graphite substrate. Line profiles taken along the scan direction give small height differences between the molecules and the substrate (a corrected apparent height of 1.31 Å),[81] evidence that there is only one adsorbed layer. Energetic considerations and theoretical results also support this claim (see Discussion below).

UHV−STM experiments reveal the presence of a second type of self-assembled monolayer for chrysene on graphite. The 20 nm by 20 nm STM image of this monolayer (Figure 1b) shows an entirely different packing structure as compared with the 20 nm by 20 nm STM image of the low-density assembly (Figure 1a). There are no large cavities or places where bare graphite is clearly observed, suggesting high-density coverage. Without additional image processing, it is not entirely obvious how the individual molecules are aligned in this high-density assembly. The pattern observed in the STM image shows a well-ordered lamellar structure, as indicated by the yellow arrows in Figure 1b. It is likely that this high-density layer is not commensurate with the underlying graphite lattice, and thus Moiré effects may be present thereby complicating the image. A Fourier transform autocorrelation analysis (Figure 2) performed on the high-density STM image (Figure 1b) indicates that the unit cell parameters are 0.80 nm by 1.23 nm and $\alpha = 80°$, roughly the size of a single chrysene molecule. Line profiles taken along the scan

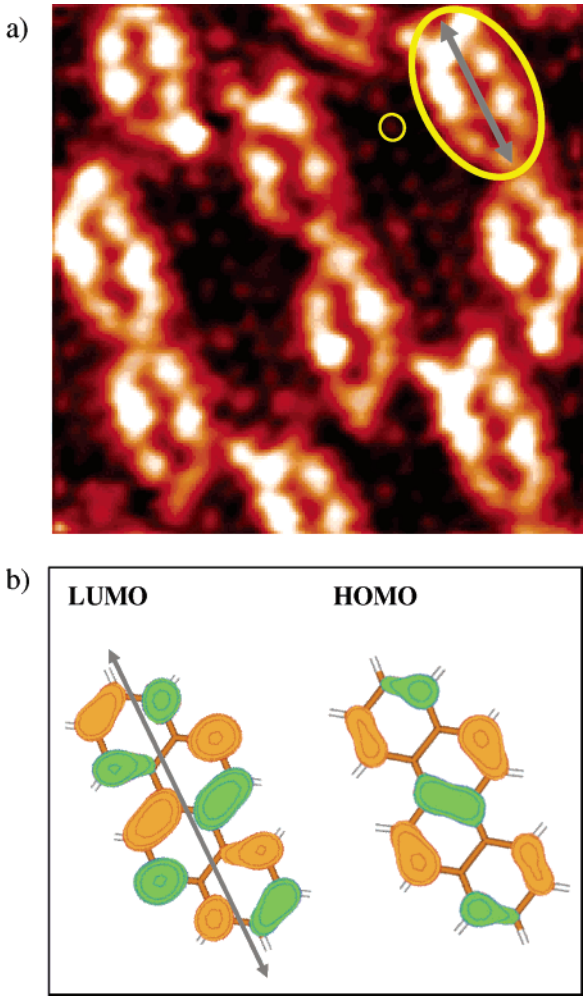

Figure 3. Comparison of a (a) 5 nm by 5 nm STM image of chrysene on HOPG with (b) the B3LYP/lacvp calculated LUMO and HOMO electronic wave functions of chrysene. The STM image (a) was obtained at +1.85 V, 90 pA, 6 Hz, with active drift control. Individual chrysene molecules (one molecule is shown within the large yellow circle) exhibit a nodal structure that is characteristic of the electronic state(s) mediating the tunneling process. In the spaces between molecules, the bare HOPG tunneling signature is observed. The small yellow circle shows a single graphite atomic spot. The calculated electronic wave function (b) for the LUMO shows a nodal plane through the center of the molecule (marked by the arrow), while a central lobe is observed in the wave function for the HOMO.

direction indicate a corrected apparent height of 1.46 Å.[82] Both the periodicity and line profile data suggest that the molecules in this high-density assembly are lying flat on the graphite surface. A high-density monolayer structure consistent with the unit cell is considered in the Theory section.

High-resolution STM images of chrysene in the low-density configuration (Figure 3a) show an interesting nodal pattern, suggesting that the images may reflect the local density of a specific electronic state/molecular orbital rather than simply the topography of the molecule. The DFT calculated frontier molecular orbitals for a single chrysene molecule in a vacuum are shown in comparison with the high-resolution STM image in Figure 3. The lowest unoccupied molecular orbital (LUMO) has a nodal plane across the center of the molecule, while the wave function for the highest occupied molecular orbital (HOMO) exhibits a central lobe. These differences should be easily discerned via STM. Indeed, the STM image obtained with positive surface bias voltage (Figure 3a) clearly resembles the calculated LUMO wave function (Figure 3b). Under positive

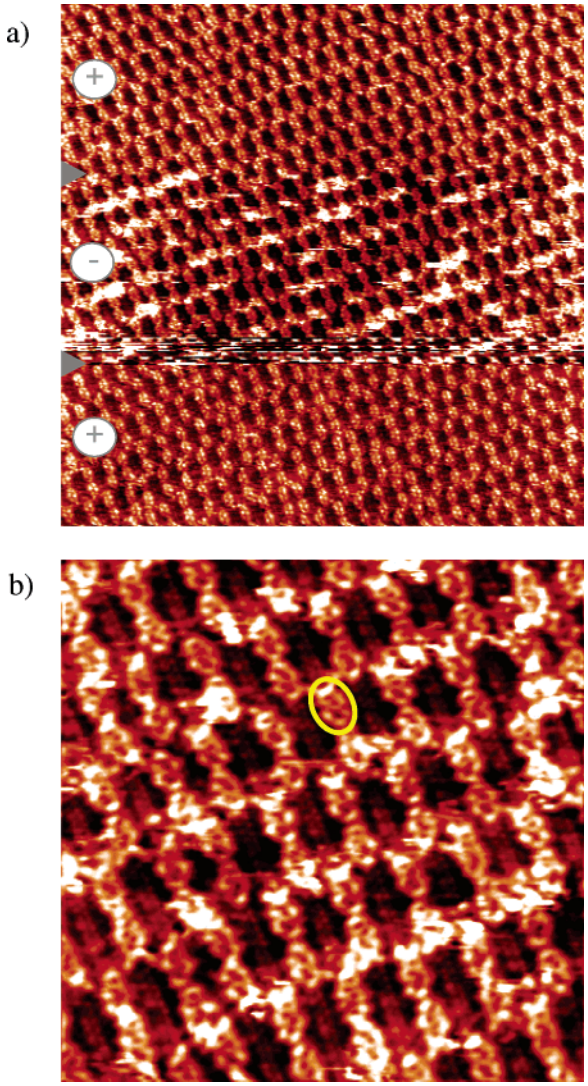

Figure 4. (a) A 50 nm by 50 nm STM image of chrysene on HOPG where the polarity (+ or −) of the voltage bias is switched during an individual frame, showing that the changes observed with polarity are reproducible. The arrowhead indicates where the polarity was switched. (b) A 15 nm by 15 nm STM image of chrysene on HOPG taken under negative polarity conditions (−1.80 V, 85 pA, 7 Hz, with active drift control). One chrysene molecule is shown within the yellow circle. Under negative polarity conditions, a change in the nodal pattern of the chrysene molecules occurs and resembles the calculated HOMO wave function (Figure 3b).

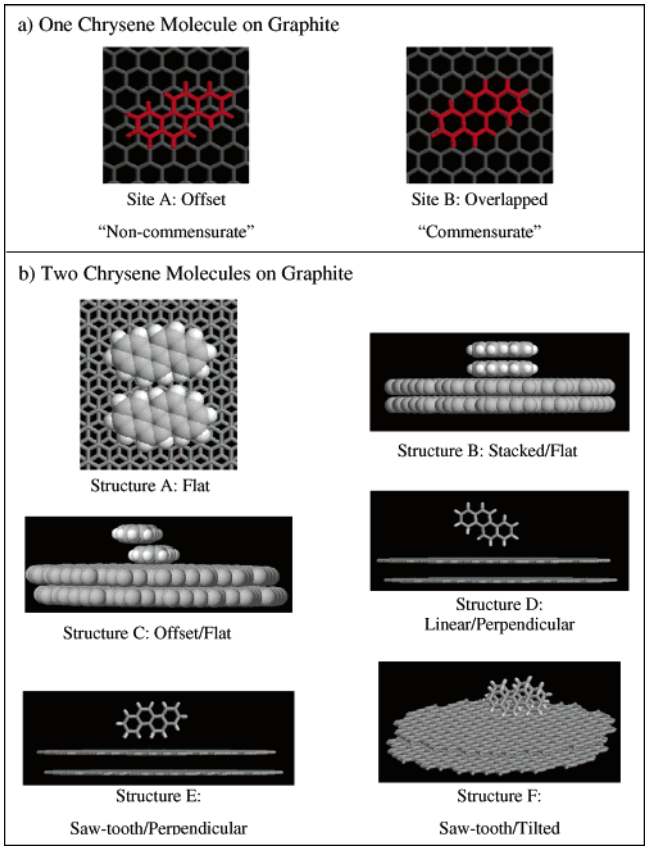

Figure 5. Comparison of several energy-minimized structures for (a) one and (b) two chrysene molecules adsorbed on graphite, calculated as described in the text. One chrysene molecule (a) can be adsorbed onto two distinct stabilization sites on graphite, site A where the chrysene molecule is offset from the underlying graphite and site B where the chrysene is aligned with the graphite rings. In part a, only the top layer of graphite is shown. For two chrysene molecules on graphite (b), several structures have been considered. Structure A has two molecules lying flat next to each other on the surface. Structure B shows two molecules π-stacked directly on top of each other on the graphite. Structure C has the molecules stacked in an offset fashion (analogous to two graphite sheets) but still flat on the surface. Structures D and E are similar configurations in which the π-stacked dimer (two molecules directly on top of each other as in B) is adsorbed perpendicular to the graphite via edge−face interactions. The perpendicular structures (D and E) differ only in the amount of rotation of the dimer relative to the graphite surface. Structure F shows a tilted alignment of the two molecules with respect to the chrysene surface. In part b, only two layers of graphite are shown for each structure.

surface bias conditions, electrons tunnel from filled states of the tip into empty states of the surface. Because of the diffuse nature of the LUMO and other unfilled states of the molecule, they are likely to dominate the tunneling process under positive surface bias conditions because other states, such as the HOMO and HOMO−1, are already filled.[4] Images taken under negative surface bias polarity show a different nodal pattern (Figure 4b). This nodal pattern more closely resembles the HOMO wave function (Figure 3b), where there is a lobe through the center of the molecule. The effect is reversible (Figure 4a), such that alternating the bias polarity during a single STM frame effectively switches between tunneling that is mediated by either the LUMO (positive surface bias) or HOMO (negative surface bias). It does not matter in which order the image is taken, positive/negative/positive (Figure 4a) or negative/positive/negative (not shown).

II. Chrysene: Theory. To determine if there is a preferred binding site for chrysene on graphite and to evaluate packing structure energetics, simulations were performed in which a single molecule was adsorbed and allowed to minimize freely on a graphite surface. The resultant configuration is one where the chrysene is offset from the underlying graphite, in a manner that is similar to the offset observed between alternating graphene sheets (Figure 5a). This offset configuration, designated site A, is compared to an alternative configuration where the chrysene molecule is overlapped with the underlying graphite, denoted site B (Figure 5a). Upon minimization of the total potential energy, molecules initially placed at site B converge to the lower-energy configuration at site A. The energetics of a single chrysene molecule adsorbed at sites A and B are given in Table 1, where the energy breakdown reported for site B is that prior to structural optimization. It is important to recognize that an isolated chrysene molecule in a vacuum has some strain energy, as indicated by the nonzero internal stretch, bend, and torsional energies. A single molecule also has a positive, unfavorable Lennard-Jones contribution to

TABLE 1: Calculated Energies (kcal/mol) of a Single Chrysene Molecule Adsorbed on Graphite at Two Distinct Stabilization Sites

interaction[a]	site A: offset[c]	site B: overlapped[c,d]
total potential Energy[b]	−9.83	−9.42
stretch	2.52	2.52
bend	1.81	1.81
torsion	0.04	0.04
electrostatic	−2.41	−2.41
Lennard-Jones	20.40	20.40
Steele	−32.18	−31.78

[a] All interaction energies are defined in the Methods section. [b] The total potential energy is the sum of the intramolecular energy (stretch, bend, torsion, and Lennard-Jones) and intermolecular energy (electrostatic, Lennard-Jones, and Steele) for a single chrysene molecule on graphite. [c] Corresponding structure is shown in Figure 5a. [d] The energies given are for the starting configuration because upon energy minimization site B converges to site A.

the total energy due to repulsive interactions between atoms within a single molecule separated by more than three bonds (1−4 atomic interactions). Adsorption of a single chrysene molecule on graphite results in an adsorbate−substrate Steele interaction that is both attractive (negative energy) and large in magnitude. The difference in energy between the two binding sites (0.41 kcal/mol) is due entirely to changes in the Steele interaction energy between the adsorbate and substrate, with site A being the preferred configuration.

When possible two-dimensional packing assemblies are considered, it is sometimes useful to refer to the structure of the molecule in the solid state.[37] The three-dimensional crystal structure for chrysene shows that the molecules stack in an offset manner in each dimension, and edge−face interactions are present between layers of the crystal.[83,84] The X-ray crystal structure for chrysene resembles those for most other PAHs, including that of pentacene.[85] Truncation of a three-dimensional crystal into two dimensions might suggest that edge−face interactions would play an important role in the structure of the physisorbed monolayer on graphite. Such edge−face interactions would only be possible when the chrysene molecules are rotated to some degree off of the graphite; however, the experimental results indicate that the chrysene molecules are likely lying flat on the surface.

Calculations performed for two chrysene molecules on graphite also address the question of how the molecules are oriented relative to the graphite surface and each other. On the basis of previous calculations on gas-phase benzene dimers[86] as well as other aromatic molecules,[87] it can be predicted that multiple ring arene systems will always favor a flat but shifted stacking motif, as is seen in the flat orientations of the chrysene molecule on the graphite "multiple ring" surface (see Figure 5a, site A). The energy-minimized structures of six possible configurations for two molecules adsorbed on graphite are shown in Figure 5b. The breakdown of the energetics for each dimer structure (A−F) on graphite is shown in Table 2. To compare the interaction energies of each dimer pair, it is useful to calculate the pair interaction or stabilization energy (E_{stab}) of the system. For structures A, D, and E, where both molecules contact the surface in identical fashion, E_{stab} is obtained by taking the energy of twice a single molecule on graphite in each configuration and subtracting this from the total energy for the interacting dimer pair. For cases where the two molecules in the pair are not in identical configurations (B, C, and D), the energies of each molecule from the dimer calculated in isolation were added together, and the sum was subtracted from the dimer interaction energy, giving E_{stab}.

Only two of the six dimers (A and C) are predicted to be stable minima when adsorbed on graphite, as indicated by a negative total potential energy (adsorbed). Structure A, where both molecules are lying side-by-side and flat on the graphite, is by far the most stable configuration for two chrysene molecules on graphite due to the highly favorable interaction between the molecules and the substrate exhibited by the large, negative Steele adsorption energy. As expected, the Steele energy for structure A is almost double that for configurations where only one chrysene molecule is in direct contact with the substrate (B and C). While the adsorbate−substrate interaction is further diminished for structures where the molecules are angled out of the plane of the graphite by 60 to 90° (D−F), the Lennard-Jones intermolecular energy is significantly lowered and more favorable for all of the other configurations (B−F) due to the attractive π-stacking interactions between the two chrysene molecules enabled by the close proximity of the chrysene pair in these configurations. The stabilization of each of the possible structures is due to both packing and adsorbate−substrate interactions, as seen in Table 2. The total energy is a result of a competition between adsorbate−substrate and adsorbate−adsorbate van der Waals interactions, with the surface interaction overwhelmingly dominant. The largest stabilization observed upon dimerization is seen in structures C and F, which exhibit the most favorable pair interaction energies (E_{stab}) of −8.71 and −8.92 kcal/mol, respectively. These structures have their chrysene molecules arranged in a similar staggered, offset way relative to each other. As stated previously, this staggered arrangement is the optimum geometry for dimers of aromatic molecules.[86,87] The offset geometry

TABLE 2: Comparison of the Calculated Energies (kcal/mol) of the Different Arrangements for Two Chrysene Molecules on Graphite

interaction[a]	A[e]	B[e]	C[e]	D[e]	E[e]	F[e]
total potential energy (adsorbed)[b]	*−21.01*	1.38	*−0.34*	15.86	8.77	5.81
stretch	5.03	5.03	4.93	4.99	5.21	9.61
bend	3.60	3.61	3.63	3.52	3.56	3.49
torsion	0.07	0.07	0.01	0.03	0.15	0.71
electrostatics	−3.99	0.77	−4.07	0.59	0.22	−1.95
Lennard-Jones	38.43	27.69	31.06	27.85	28.07	26.02
Steele	−64.15	−35.80	−35.99	−21.12	−28.44	−32.08
total potential energy (isolated)[c]	43.14	37.17	36.65	36.98	37.21	37.88
pair interaction energy (E_{stab})[d]	−1.68	−7.53	−8.71	−7.66	−7.57	−8.92

[a] All interaction energies are defined in the Methods section. [b] Total interaction energy of each dimer in the presence of the substrate. Those entries shown in italics are stable configurations for two chrysene molecules adsorbed on graphite. [c] Total energy for each chrysene dimer optimized in a vacuum without the graphite substrate. [d] Pair interaction energies (stabilization energies) for each dimer configuration are calculated as the total interaction energy for the dimer on graphite corrected for the energy of the individual chrysene molecules on graphite in the same configuration as the dimer. [e] Corresponding structures are shown in Figure 5b.

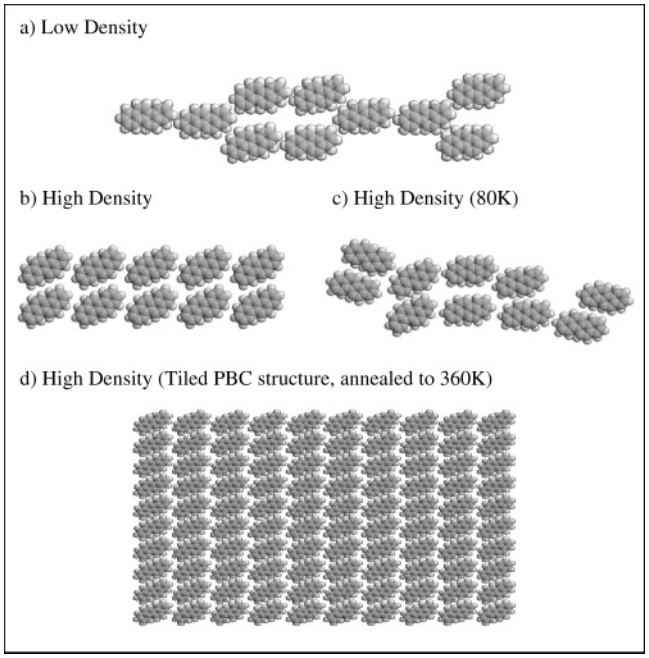

Figure 6. Comparison of the energy-minimized configuration (calculated as described in the text) for 10 chrysene molecules on graphite in (a) the low-density configuration observed with STM and (b) a high-density close-packed configuration. Constant NVT molecular dynamics simulations, without periodic boundary conditions, were run for the energy-minimized close-packed structure (b), and the resulting structure after 50 ps at 80 K is shown in part c. Only small structural changes are observed in part b with the addition of thermal energy when no boundary conditions are imposed (c), suggesting that part b is a favorable monolayer configuration. A one-molecule unit cell periodically replicated calculation (i.e., with periodic boundary conditions, PBC) using the structural information gleaned from the experimental and the calculated unit cell (b) is shown in part d. The PBC simulations used cell parameters of $a = 11.9$ Å, $b = 8.61$ Å, and $\alpha = \beta = \gamma = 90°$ and a smooth potential for graphite. The monolayer structure (d) is maintained upon annealing to 360 K. While chrysene itself is not chiral, chrysene adsorbed on HOPG is a pseudo-chiral system. In each optimized configuration shown, the chrysene molecules share the same chirality. In all cases, the graphite surface was included in the calculation, although it has been removed from the figure for presentation purposes.

results in overall net favorable $\pi-\pi$ interactions because it maximizes the favorable $\pi-\sigma$ interactions while minimizing the repulsive $\pi-\pi$ interactions between the molecules.[87] This correlates well with the results of Table 1, which show that the chrysene molecules prefer to bind offset from the underlying graphite layer (Figure 5a, site A). In fact, structures C and F are dimers that behave as miniature pieces of graphite, where interacting graphene sheets exhibit an offset between the layers. While such tilted configurations as structures C and F might become important in the high-coverage or multilayer limit, the experimental conditions are such that the surface coverage for chrysene on graphite is in the monolayer or even sub-monolayer regime where adsorbate−substrate interactions likely drive the self-assembly into configurations in which the molecules lie flat on the surface.

To determine the driving forces for self-assembly and the origin of at least two distinct packing assemblies observed in the STM images, energy minimizations for larger sets of chrysene molecules on graphite have also been performed. A summary of the energetics for 10 chrysene molecules adsorbed on graphite in a low-density configuration (Figure 6a) and a high-density configuration (Figure 6b) is presented in Table 3.

The low-density monolayer configuration observed by STM (Figure 1a) is easily modeled using a patch of 10 chrysene molecules on graphite as shown in Figure 6a. The energy-minimized low-density structure (Figure 6a) accurately reproduces the experimentally determined cavity dimensions; the calculated values for *a* and *b* are 2.3 and 0.4 nm, respectively, as compared to the experimentally measured values of 2.2 and 0.5 nm, respectively.

TABLE 3: Comparison of the Calculated Energies (kcal/mol) for 10 Chrysene Molecules on Graphite in Two Distinct Configurations

interaction[a]	HD[b]	LD[b]	ΔE HD[c]	ΔE LD[c]
total potential energy	−108.59	−103.52	−10.27	−5.20
stretch	25.24	26.42	0.08	1.26
bend	17.96	18.00	−0.09	−0.05
torsion	0.38	0.35	0.03	0.00
electrostatic	−16.81	−18.84	7.27	5.25
Lennard-Jones	184.69	190.99	−19.36	−13.06
Steele	−320.04	−320.44	1.81	1.41

[a] All interaction energies are defined in the Methods section. [b] Two different 10-molecule clusters were modeled: high-density (HD) and low-density (LD) monolayer configurations. Corresponding structures are shown in Figure 6. [c] Stabilization energies for the two clusters (ΔE HD, ΔE LD) are calculated as the difference in energy between the 10-molecule cluster and 10 times the energy of a single chrysene molecule on graphite in the lowest-energy stabilization site (site A from Table 1, Figure 5a).

Possible structures for the high-density packing assembly have been assessed using molecular modeling and simple geometric packing considerations. Only structures in which the molecules are lying completely flat on the graphite surface are considered feasible for the high-density assembly, in keeping with the STM images and the dimer calculations (Table 2). One structure consistent with features observed in the STM images and the Fourier transform analysis (Figure 2) has been analyzed using the aforementioned theoretical methods, the results of which are detailed below.

The high-density structure observed by STM (Figure 1b) is probably the result of molecules assembling in a close-packed configuration such as the energy-minimized structure shown in Figure 6b. This configuration is the only one consistent with the unit cell parameters determined by the Fourier transform autocorrelation analysis (Figure 2). In this configuration, the stabilization energy (ΔE HD) for the 10-molecule cluster is −10.27 kcal/mol (Table 3), indicating that each chrysene molecule is stabilized by ∼1 kcal/mol as compared to 10 noninteracting, separated chrysene molecules on graphite (in site A from Figure 5a). This type of assembly pattern shares many of the characteristics observed in the STM image (Figure 1b) and the Fourier transform analysis (Figure 2), including lamellae in two dimensions separated by an angle of ∼80°. Molecular dynamics simulations were performed for the high-density structure at 80 K, the temperature at which the images were obtained. Much of the energy-minimized structure is maintained at 80 K (Figure 6c), despite the fact that no boundary conditions have been imposed, indicating that this is a favorable structure even upon introduction of thermal energy. The high-density structure was then simulated under two-dimensional periodic boundary conditions (PBC), using a one-molecule unit cell with dimensions taken from the previous minimizations ($a = 11.9$ Å, $b = 8.61$ Å, and $\alpha = \beta = \gamma = 90°$). A smoothed-out graphite surface was used for this set of periodic simulations (i.e., only the first term in the Steele potential was included).[77] Leaving out corrugation is necessary to maintain a correct and consistent matching of the periodicities between the substrate and adsorbate models. The structure remained stable and flat and maintained the relative intermolecular configuration seen

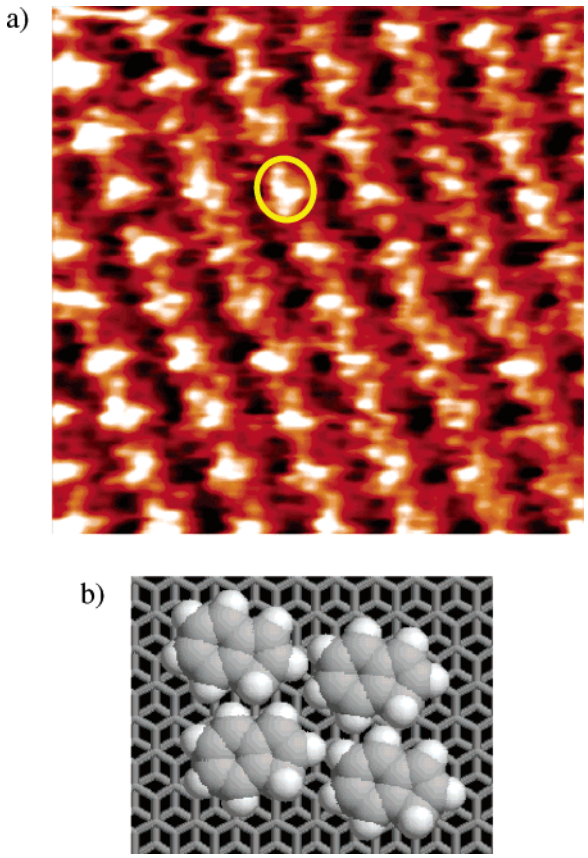

Figure 7. (a) A 5 nm by 5 nm portion of an STM image of indene on HOPG. The image was obtained at +2.00 V, 100 pA, and a scan rate of 7 Hz. The image has been processed using a first-order Fourier transform low-pass Butterworth filter with a large cutoff frequency. The indene molecules form a well-ordered lamellar assembly. Each cluster of bright spots, indicated by a yellow circle, corresponds roughly to the size of one indene molecule (0.68 nm × 0.50 nm). (b) The energy-minimized structure of four indene molecules on graphite calculated as described in the text.

in the unbounded simulations, even after annealing up to the experimental temperature of 360 K. A large tiled patch of the high-density structure obtained after the annealing schedule of 50 ps at 360 K, followed by cooling to 325, 300, 275, 250, etc. all the way down to 80 K is shown in Figure 6d.

To begin to understand why two distinct monolayer structures are observed experimentally for chrysene on graphite, it is useful to look at the breakdown of the energetics for the energy-minimized low-density and high-density structures of 10 chrysene molecules on graphite (Table 3, Figures 6a and 6b). The total potential energy of each 10-molecule set is favorable when compared to 10 times the energy of a single chrysene molecule in the flat configuration (structure A) on graphite. Specifically, the high-density structure is stabilized by 10 kcal/mol, while the low-density one gains 5 kcal/mol. The high-density structure is preferred over the low-density assembly in that it allows more molecules to pack per unit area on the graphite surface. The calculations also indicate that the high-density structure is preferred on a per molecule basis and thus should be preferred for any coverage. The large, favorable (negative) Steele energy is the interaction term contributing most to the total potential energy for all structures. Not surprisingly, the intermolecular Lennard-Jones interactions between molecules are more favorable by over 6 kcal/mol when molecules are packed more densely, as in the high-density structure, due to the short-range nature of this interaction. Despite its overall higher total potential energy, the low-density structure is able to minimize the unfavorable electrostatic interactions among the molecules by 2 kcal/mol as compared to the high-density one. However, this small gain in energy by minimizing repulsive electrostatic forces does not compensate for weaker intermolecular Lennard-Jones interactions in the low-density structure as compared to the high-density one. The play-off between repulsive electrostatic forces and attractive Lennard-Jones forces ultimately favors a high-density assembly over a low-density one.

TABLE 4: Comparison of the Calculated Energies (kcal/mol) for the Minimized Structure of Four Indene Molecules Adsorbed on Graphite as Compared to a Single Indene Molecule on Graphite

interaction[a]	four[b]	one[b]	ΔE[c]
total potential energy	−1.94	0.60	−4.34
stretch	1.57	0.37	0.09
bend	71.67	17.91	0.03
torsion	−1.26	−0.32	0.00
electrostatic	−16.32	−4.34	1.02
Lennard-Jones	10.07	3.92	−5.61
Steele	−67.67	−16.95	0.12

[a] All interaction energies are defined in the Methods section. Upon the basis of the STM image (Figure 7a), a four-molecule indene cluster on graphite ("four") and a single indene molecule on graphite ("one") were individually optimized. The four-molecule cluster on graphite is shown in Figure 7b. [c] Stabilization energies for the cluster (ΔE) are calculated as the difference in energy between the four-molecule cluster and 4 times the energy of a single indene molecule on graphite in the lowest-energy configuration.

Because the STM images are consistent with assemblies where the chrysene molecules are lying flat on the graphite substrate, configurations where 10 molecules are oriented in a perpendicular or tilted arrangement on the substrate have not been considered in the present analysis. Upon the basis of calculations of two chrysene molecules on graphite (Table 2), it is energetically much less favorable for chrysene molecules to adsorb via edge−face interactions as opposed to lying flat in the plane of graphite. The presence of beneficial intermolecular interactions for a full monolayer of molecules packing in a tilted or perpendicular configuration might be substantial enough to outweigh the loss of adsorbate−substrate interactions arising from rotation of the chrysene molecules off the graphite surface into the vacuum. However, this is clearly not the case for two chrysene molecules, and the experimental data does not support perpendicular or tilted structures.

III. Indene: UHV−STM and Theory. A 5 nm by 5 nm portion of a STM image of indene adsorbed on the basal plane of graphite is shown in Figure 7a. Indene forms well-ordered lamellae on the graphite substrate. The lamellae have an average width of 0.70 nm, consistent with the expected width of a single indene molecule (0.68 nm). Within a given lamella, clusters of "bright" spots are observed with a spacing of about 0.58 nm. Each cluster is assigned to a single indene molecule. A possible assembly pattern matching the measured geometric factors is shown in Figure 7b. This is the energy-minimized structure for four indene molecules on graphite. The energy breakdown for the cluster compared with that of a single indene molecule adsorbed on graphite is listed in Table 4.

Discussion

I. Observation of Small PAHs on Graphite with STM. Direct observation of the self-assembly of the small PAHs chrysene and indene on graphite is remarkable. Unlike previous STM studies at the liquid−graphite[1,3−5,8−10,18,21,28,31−41] and vacuum−graphite[23−25,42−46] interfaces, the molecules studied here are of relatively low molecular weight and contain no alkyl

chains, polarizable headgroups, or hydrogen-bonding sites known to promote self-assembly. The primary driving force for self-assembly is the favorable interaction between the adsorbate and the substrate. Favorable but weak van der Waals interactions between neighboring absorbate molecules will also contribute to the spontaneous self-assembly of these small PAHs on graphite.

Theoretical studies of these adsorbates on graphite surfaces provide a guide with which to interpret the self-assembly of chrysene and indene at a quantitative level. From the calculations, the total potential energy of a given packing structure can be dissected to determine those factors (e.g., adsorbate−substrate interactions, adsorbate−adsorbate interactions) that drive the self-assembly in each case.

A. Chrysene. While the calculations for a single chrysene molecule on graphite suggest that there is a preferred stabilization configuration (Figure 5a, site A), the energy difference between the possible stabilization sites is quite small and well within *kT* at the annealing temperature used in these experiments. With only van der Waals forces between the adsorbate and substrate, as is the case for chrysene on graphite, the barriers to motion parallel to the surface are expected to be on the order of 0.3−1 kcal/mol.[88] Given the small barrier to translation from one site to another, the molecules can sample each site upon deposition and during annealing. This lack of a significant barrier to translation between adsorption sites may be the cause of the large number of defects observed for the low-density structure (Figure 1a), where the defect appears as a significant decrease in the spacing between molecules within a given lamella, an example of which is labeled *c* in Figure 1a. Furthermore, the observation of a commensurate (low-density) and noncommensurate (high-density) structure indicates that practically speaking there is no unique stabilization site for chrysene on graphite.

The theoretical studies of the two-molecule clusters (Table 2, Figure 5) suggest that in a vacuum the chrysene molecules prefer to lie flat on the graphite surface (structure A) rather than π-stacking with each other (structures B−F) and interacting with the surface through edge−face interactions (structures D−F). While structure A, with two chrysene molecules side-by-side on the graphite, is the least favorable with respect to optimization of the intermolecular van der Waals (Lennard-Jones) energy, this structure ultimately displays the most favorable total energy when bound to the surface and is most likely the only one observed experimentally in this study. In structure A, both molecules lie completely flat on the surface, thereby maximizing the adsorbate−substrate interactions in contrast to the out-of-plane configurations (structures B−F). The adsorbate−substrate interaction drives the self-assembly toward a flat configuration, despite the fact that the adsorbate intermolecular Lennard-Jones interactions are significantly less favorable when the molecules are side-by-side versus π-stacked.

It should be noted that while suggestive this two-molecule analysis is not conclusive. Perpendicular or tilted structures such as those depicted in D−F of Figure 5b may become relevant in the high-coverage (multilayer) limit. However, on the basis of previous work on organic layers on graphite,[23] the surface preparation conditions utilized in the present study are such that deposition is in the low-coverage (monolayer/sub-monolayer) regime. In such a low-coverage limit, the molecules would prefer to lie flat, thereby substantially increasing their interaction energy with the surface at the expense of their interaction with each other. Both the high- and low-density packing assemblies observed in the present work occur for chrysene on graphite under monolayer/sub-monolayer surface coverage conditions. The theoretical results and the STM images indicate that both the high- and low-density configurations are assemblies in which the chrysene molecules lie flat on the graphite surface.

Observation of two types of assembly structures via STM reflects the rough, multiwell nature of the global potential energy surface of the chrysene−graphite system. The minimizations indicate that the energy difference between the two assigned configurations (high- and low-density) is ∼5 kcal/mol for 10 molecules, almost 7 times larger than the available thermal energy (0.75 kcal/mol) at the annealing temperature used in the experiments. Presumably there are numerous configurations not considered here that represent metastable minima on the potential energy surface for chrysene on graphite. The high-density domain observed with STM (Figure 1b) and assigned to the calculated high-density structure (Figure 6b) is likely one of the lowest-energy, or perhaps even the global minimum, packing configurations for chrysene on graphite, as energy per unit area is minimized in such a close-packed structure.

The observation of both low- and high-density assemblies, despite identical deposition and annealing conditions (within ±5 K), suggests that trapping of high-energy assemblies can occur with a significant barrier to rearrangement into a lower-energy configuration. Such a kinetic component to the self-assembly may exist making it difficult to achieve the lower-energy, high-density configuration on the time scale of the experiments. One such potential kinetic constraint due to a geometric effect (chirality) will be discussed in detail below.

While entropy has not been included in the theoretical analysis to date, it will also play a role in the self-assembly process. The observation of both a low- and high-density monolayer structure for chrysene on graphite may indicate a competition between entropy and enthalpy as the primary driving force for the self-assembly process. Entropy may favor a low-density structure in which there are fewer chrysene molecules that can sample multiple stabilization sites on the graphite surface. The modeling presented above suggests that enthalpy favors a high-density structure with more molecules packed per unit area on the graphite surface.

Finally, it is plausible that two different packing structures are observed for the self-assembly of chrysene on graphite due to experimental, coverage-dependent self-assembly. While the experimental conditions were carefully controlled and identical within the error associated with measuring the temperature of the chrysene sample during vapor deposition and the graphite substrate during annealing, small changes in conditions could result in dramatically different amounts of chrysene being present on the graphite during different experimental runs. Thus the molecules may adopt one configuration at low coverage and another at higher coverage, corresponding to low- and high-density structures, respectively. However, this scenario seems unlikely considering that each configuration was observed multiple times and the error associated with the temperature measurements is quite small.

B. Indene. Indene is perhaps the smallest aromatic so far observed via STM to self-assemble on graphite in UHV. Smaller molecules, such as *n*-alkanes and halo-alkanes,[45] which exhibit very strong dispersion interactions between the alkyl chains and headgroups, are known to self-organize and have been observed with the STM. Other small aromatics, such as trimesic acid,[46] are also known to self-assemble on graphite, but these molecules form very strong hydrogen-bonded networks that dominate the self-assembly. The absence of any large self-assembly forces in the case of indene hints at the importance of subtle interactions, involving short-range and weak forces, that drive

the self-assembly. The presence of one saturated carbon on the five-membered ring allows for an increased adsorbate−substrate interaction as one of the hydrogen atoms points down into the graphite. Thus, the indene is likely to be held more closely to the graphite surface than a flat analogue would be. This interaction is similar to the interaction between methylene units and the underlying graphite in the case of self-assembly by alkanes.[3,4,7]

The calculations indicate that the main driving force for self-assembly of indene on graphite is the absorbate−substrate van der Waals (Steele) energy (Table 4). While the adsorbate−substrate energy dominates, the weak van der Waals interactions between molecules also contribute favorably to self-assembly. It should be noted that a single indene molecule has a considerable internal energy, most likely due to ring strain associated with a fused five- and six-membered ring structure. While the magnitude of this energy might be overestimated in the current harmonic simulations, the relative energy of the cluster versus that of an equivalent number of single molecules is not expected to be altered by this internal energy. Indeed, the stretch, bend, and torsional components completely cancel out when determining the stabilization energy of the cluster (ΔE in Table 4).

II. Chrysene on Graphite: A Pseudo-Chiral System. While chrysene itself is not chiral, chrysene adsorbed on graphite is pseudo-chiral. The two distinct adsorbate structures are shown below. Adsorption of the molecule on graphite is expected to be equally probable for each "enantiomer" as the surface−molecule interactions are identical for each orientation.

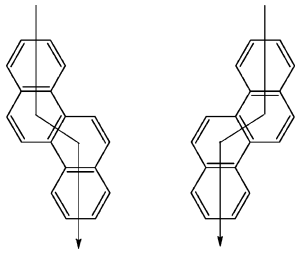

The chirality of the molecules on the surface can be determined by close inspection of the low-density monolayer structure STM image for chrysene (Figures 1a and 3a) and comparison with the calculated LUMO (Figure 3a). The wave function of the LUMO is concentrated along the perimeter of chrysene, showing a large nodal plane through the center of the molecule. This central node follows the shape of the chrysene "step" as noted by the arrows in the structures above and observed in Figures 1a and 3a. For all STM topographs collected, the low-density monolayer has nearly equal amounts of each adsorbate enantiomer present. For example, in the STM topographic image shown in Figure 1a there are 69 right-handed enantiomers and 67 left-handed ones. While adsorbates of the same chirality tend to group in small regions, there is clearly no enantiomeric segregation. This is unlike the segregation observed previously for chiral and pseudo-chiral self-assembled monolayers at the liquid−graphite interface.[31,39−41]

To model a high-density structure in which the molecules are all lying flat on the substrate, geometric constraints for packing as many molecules as possible on the surface dictate that the adsorbate molecules maintain identical chirality. However, the presence of chirality is not obvious in the chrysene high-density assembly based on inspection of the STM topograph shown in Figure 1b. While experiments performed at the liquid−graphite interface have shown segregation based on chirality,[31,39−41] the dynamic equilibrium established between molecules on the surface and molecules in solution presents a low-energy pathway decreasing the barrier to out-of-plane movement of the surface adlayers. Furthermore, these liquid−solid interface experiments are typically performed near room temperature, which makes the possibility of an equilibrium among multiple, stable surface structures more likely. Under the current low-temperature, UHV conditions, adsorbate chirality may provide a kinetic "bottleneck" for the self-assembly of chrysene into the energetically preferred high-density configuration, thereby explaining the observation of the low-density structure. Assuming equal sticking probability for each enantiomer upon deposition, formation of domains having molecules all oriented with the same chirality and packed tightly requires diffusion of chrysene molecules across the surface to form chirally segregated domains or enough energy to lift a molecule off the surface and flip it over. Diffusion of chrysene across large areas of graphite is likely to be slow and may require concerted motions of the molecules. Alternatively, rotation of the molecules out of the plane of the surface would require overcoming the large dispersion interaction between the molecule and the surface (the Steele energy), the energetic cost of which is comparable to complete desorption. Because the present experiments are performed at the vacuum−graphite interface, the barrier to rotation of a chrysene molecule is expected to be quite large. Once the substrate is cooled below room temperature for analysis via STM, the molecules are essentially locked into position and have only a small amount of vibrational motion. This suggests that the low-density structure is metastable in agreement with the theoretical model calculations and that the high-density structure, if it is chiral, likely arises in samples where sufficient numbers of molecules are deposited under conditions where annealing is complete enough to allow surface diffusion and/or molecular flipping.

Because the adsorption of one enantiomer is not expected to be energetically preferred over the other, large domains comprised of either one enatiomer or the other are likely to exist on the graphite surface. Due to the presence of the complicating Moiré effect for the high-density structure, determining exactly which enatiomer is observed in Figure 1b is difficult. Thus far, grain boundaries between domains have been observed; however it is unclear if such domains represent different chiralities. A future investigation of the structural properties (e.g., grain boundaries, point defects) of such pseudo-chiral systems will be extremely interesting from both an experimental and a theoretical perspective.

III. Electronic Structure and Tunneling Mechanism for Chrysene on Graphite. The observation of distinct STM topographic images for chrysene upon alternating the bias voltage polarity is indicative of the presence of two or more molecular electronic states that dominate tunneling into and out of the substrate. The STM topographs of chrysene resemble the DFT calculated LUMO when electrons tunnel from the tip to the surface ($+V_{sample}$, Figures 1a and 3a) and the HOMO when electrons tunnel from the surface to the tip ($-V_{sample}$, Figure 4b). Orbital-mediated tunneling such as this has been observed previously in the bias dependence of the tunneling current for monolayers of molecules such as the PAH coronene,[24] porphyrin derivatives,[89−91] donor−acceptor molecules,[34] and naphthalocyanine[23] on metal or semimetal surfaces.

To understand the tunneling mechanism for chrysene on graphite, it is useful to consider the electronic energy level structure of the molecule with respect to that of the substrate.[4,89] In the absence of definitive experimental data relating the energy

TABLE 5: Becke3LYP/lacvp Calculated Energy Differences (eV) between Selected Electronic States of an Isolated Chrysene Molecule in Vacuum

electronic states	ΔE
HOMO − LUMO	4.25
LUMO − [LUMO+1]	0.42
HOMO − [HOMO−1]	0.52
[HOMO−1] − [HOMO−2]	0.45

of the HOMO and LUMO of the molecular adsorbate to the Fermi level of the graphite, as might be obtained via ultraviolet photoelectron spectroscopy, several approximate methods can be used. The simplest assumes that the HOMO−LUMO gap for chrysene on graphite is equal to the DFT calculated gap for an isolated molecule (4.25 eV, Table 5). Because the chrysene molecules are only weakly coupled to the substrate via van der Waals interactions, the energies of the HOMO and LUMO states for the isolated molecule are expected to be similar to those of the adsorbate molecule. The gas-phase ionization potential for chrysene is 7.60 eV.[92] With the vacuum level pinned such that the ionization potential of the molecule is aligned with the work function of graphite (4.8 eV), the HOMO and LUMO levels can be approximately located with respect to the graphite Fermi level.[4] Through use of this procedure, the chrysene HOMO is predicted to be located at about −2.8 eV, and the LUMO would be at about +1.5 eV, relative to the Fermi level of graphite. These energies are comparable to the energies of the tunneling electrons given the accessible bias voltage. Because the molecules are more strongly coupled to the surface than the tip, it is expected that their electronic-state energies track the surface potential,[89] unlike the symmetric metal−molecule−metal junction.[93,94]

An alternative approach to approximating the energy of the HOMO and LUMO states relative to the Fermi level of the substrate is to use electrochemical data for the molecule of interest.[34,90,91] The first oxidation and reduction potentials of a molecule can be related to the energy of the molecular HOMO and LUMO levels, respectively. For chrysene, the first oxidation and reduction potentials are +1.64 and −2.27 V vs SCE.[95] Through use of this electrochemical data, along with a vacuum-scale conversion factor (the zero of the SCE scale is 4.71 V below the vacuum level), the HOMO and LUMO levels can be located approximately 6.35 and 2.44 V, respectively, below the vacuum level.[90,91] By taking the work function of graphite as 4.8 eV, this electrochemical analysis predicts the HOMO and LUMO of chrysene to be at −1.55 and +2.36 V, respectively, relative to the Fermi level of graphite. Again, these energies are comparable to the energies of the tunneling electrons given the accessible bias voltage. This analysis also gives an approximate HOMO−LUMO gap of 3.91 V, consistent with that calculated using DFT.

Both analyses suggest that in the STM experiments tunneling from the tip to the surface ($+V_{sample}$) is dominated by the coupling of the chrysene LUMO to the surface. When the bias polarity is reversed, tunneling is dominated by the coupling of the chrysene HOMO to the graphite. Due to broadening of the energy distribution of electrons in the tip (which is not cooled in our apparatus), the surface−molecule coupling of other electronic states of chrysene may also contribute to the tunneling current. The contribution of these states will, of course, fall off as the energy of the chrysene states is displaced from the graphite Fermi level.

Conclusions

The present work has shown that the small, polycyclic aromatic molecules chrysene and indene can be self-assembled on graphite and interrogated by STM under low-temperature, ultrahigh vacuum conditions. These molecules form well-ordered assemblies, despite the fact that they lack any of the structural features typically associated with self-assembly (e.g., hydrogen bonding, long alkyl chains, polarizable headgroups).

For chrysene, two significantly different monolayer assembly structures were observed with STM. Possible origins for these different packing structures have been discussed in terms of a competition between entropy and enthalpy or kinetic trapping of the low-density structure due to a purely geometric effect (pseudo-chirality). It may be possible to observe experimentally the effect of thermal energy on the transformation from the low-density to the high-density structures by heating the surface allowing direct determination of the barrier to transformation between these configurations. These types of experiments are ongoing in our laboratory.

High-resolution STM topographic images of the low-density packing structure of chrysene reveal a nodal structure characteristic of the electronic wave functions involved in the tunneling process. Density functional theory calculations allow assignments of these states as the chrysene LUMO under conditions where electrons tunnel from the tip to the surface and the HOMO when electrons tunnel from the surface to the tip.

The synergy between theory and experiment in the current work has proven to be extremely powerful. Structural identification and analysis has been investigated for both chrysene and indene on graphite in a quantitative manner that does not rely simply on qualitative speculation. Energy minimization and molecular dynamics simulations have been performed on monolayer structures consistent with those observed experimentally using STM. The theoretical studies provide a picture of the driving forces for self-assembly that allows for the dissection of the total potential energy of the system into its contributing parts (e.g., van der Waals, electrostatic, adsorbate−substrate, etc.). Currently, this type of information cannot be obtained easily via experiments.

The ability to couple theoretical and experimental studies of such molecular adsorbate systems has also provided insights into the fundamental aspects of the physical and chemical properties of these systems. Future work will be focused on determining how the substrate modifies the electronic structure of the molecular adsorbate. Such information is of fundamental importance for understanding charge transport in organic semiconductors, single molecule conduction, and device preparation via a bottom-up self-assembly process.

The results presented here are also of potential importance in the study of surface reactions relevant to combustion chemistry, since graphite surfaces provide a convenient, first-order model for studying soot particle chemistry. If small PAH molecules, which are key intermediates and products in soot formation, can be identified and characterized on these surfaces using STM and theoretical methods, as has been done in the present work, then soot reaction mechanisms can be traced on a model surface such as graphite. Previous work has placed particular emphasis on formation of the first aromatic ring in soot chemistry mechanisms,[57−59] and possible pathways to initial ring formation will be investigated on graphite surfaces in future studies. Obtaining evidence for the formation of PAHs such as indene or chrysene from small precursor molecules on graphite is now possible since the STM signatures of these potential reaction products have been obtained in the present study. Surface defects and step edges are also likely to play an important role in the chemistry occurring on graphite. Though these are typically minority sites on graphite surfaces carefully

prepared for UHV work, STM, being a single molecule/single site probe technique, can be used to follow reactions occurring at these surface irregularities.

Acknowledgment. This work was funded by the Department of Energy under Grant No. DE-FG02-88ER13937 (G.W.F.) and by the National Science Foundation under Grant No. CHE-03-16896 (B.J.B.). Partial support was provided by the Nanoscale Science and Engineering Initiative of the National Science Foundation under Award No. CHE-0117752 and by the New York State Office of Technology, Science, and Academic Research (NYSTAR). Equipment support was provided by the National Science Foundation under Grant Nos. CHE-00-95649 (G.W.F.) and CHE-03-52582 (G.W.F.). G.M.F. acknowledges the support of the Dreyfus Foundation through their postdoctoral program in environmental chemistry. The authors are grateful to Dr. Kavita Kannappan for her assistance, Markus Lackinger and Lorenz Kampschulte for performing the autocorrelation analysis of the STM images, and Dr. Mark Hybertsen for stimulating discussions.

References and Notes

(1) Cyr, D. M.; Venkataraman, B.; Flynn, G. W. *Chem. Mater.* **1996**, *8* (8), 1600.
(2) De Feyter, S.; De Schryver, F. C. *Chem. Soc. Rev.* **2003**, *32* (3), 139.
(3) Buchholz, S.; Rabe, J. P. *J. Vac. Sci. Technol., B* **1991**, *9* (2), 1126.
(4) Giancarlo, L. C.; Flynn, G. W. *Annu. Rev. Phys. Chem.* **1998**, *49*, 297.
(5) Giancarlo, L. C.; Flynn, G. W. *Acc. Chem. Res.* **2000**, *33* (7), 491.
(6) Rosei, F.; Schunack, M.; Naitoh, Y.; Jiang, P.; Gourdon, A.; Laegsgaard, E.; Stensgaard, I.; Joachim, C.; Besenbacher, F. *Prog. Surf. Sci.* **2003**, *71* (5−8), 95.
(7) Rabe, J. P.; Buchholz, S. *Science* **1991**, *253* (5018), 424.
(8) McGonigal, G. C.; Bernhardt, R. H.; Yeo, Y. H.; Thomson, D. J. *J. Vac. Sci. Technol., B* **1991**, *9* (2), 1107.
(9) McGonigal, G. C.; Bernhardt, R. H.; Thomson, D. J. *Appl. Phys. Lett.* **1990**, *57* (1), 28.
(10) Claypool, C. L.; Faglioni, F.; Goddard, W. A., III; Gray, H. B.; Lewis, N. S.; Marcus, R. A. *J. Phys. Chem. B* **1997**, *101* (31), 5978.
(11) Eigler, D. M.; Schweizer, E. K. *Nature* **1990**, *344* (6266), 524.
(12) Ho, W. *J. Chem. Phys.* **2002**, *117* (24), 11033.
(13) Durr, M.; Biedermann, A.; Hu, Z.; Hofer, U.; Heinz, T. F. *Science* **2002**, *296* (5574), 1838.
(14) Hu, Z. H.; Biedermann, A.; Knoesel, E.; Heinz, T. F. *Phys. Rev. B* **2003**, *68*.
(15) Mitsui, T.; Rose, M. K.; Fomin, E.; Ogletree, D. F.; Salmeron, M. *J. Chem. Phys.* **2002**, *117* (12), 5855.
(16) Mitsui, T.; Rose, M. K.; Fomin, E.; Ogletree, D. F.; Salmeron, M. *Science* **2002**, *297* (5588), 1850.
(17) Mitsui, T.; Rose, M. K.; Fomin, E.; Ogletree, D. F.; Salmeron, M. *Surf. Sci.* **2003**, *540* (1), 5.
(18) Padowitz, D. F.; Messmore, B. W. *J. Phys. Chem. B* **2000**, *104* (43), 9943.
(19) Rim, K. T.; Fitts, J. P.; Müller, T.; Adib, K.; Camillone, N.; Osgood, R. M.; Joyce, S. A.; Flynn, G. W. *Surf. Sci.* **2003**, *541* (1−3), 59.
(20) Rider, K. B.; Hwang, K. S.; Salmeron, M.; Somorjai, G. A. *Phys. Rev. Lett.* **2001**, *86* (19), 4330.
(21) Stevens, F.; Beebe, T. P. *Langmuir* **1999**, *15* (20), 6884.
(22) Barlow, D. E.; Hipps, K. W. *J. Phys. Chem. B* **2000**, *104* (25), 5993.
(23) Lackinger, M.; Müller, T.; Gopakumar, T. G.; Müller, F.; Hietschold, M.; Floyy, G. W. *J. Phys. Chem. B* **2004**, *108* (7), 2279.
(24) Lackinger, M.; Griessl, S.; Heckl, W. M.; Hietschold, M. *Anal. Bioanal. Chem.* **2002**, *374*, 685.
(25) Lee, H. S.; Iyengar, S.; Musselman, I. H. *Langmuir* **1998**, *14* (26), 7475.
(26) Nicoara, N.; Custance, O.; Granados, D.; Garcia, J. M.; Gomez-Rodriguez, J. M.; Baro, A. M.; Mendez, J. *J. Phys.: Condens. Matter* **2003**, *15* (38), S2619.
(27) Qiu, X. H.; Nazin, G. V.; Ho, W. *Science* **2003**, *299* (5606), 542.
(28) Samori, P.; Rabe, J. P. *J. Phys.: Condens. Matter* **2002**, *14* (42), 9955.
(29) Toerker, M.; Fritz, T.; Proehl, H.; Sellam, F.; Leo, K. *Surf. Sci.* **2001**, *491* (1−2), 255.
(30) Mazur, U.; Hipps, K. W. *J. Phys. Chem.* **1995**, *99* (17), 6684.
(31) Fang, H. B.; Giancarlo, L. C.; Flynn, G. W. *J. Phys. Chem. B* **1998**, *102* (38), 7311.
(32) Gesquiere, A.; Abdel-Mottaleb, M. M.; De Feyter, S.; De Schryver, F. C.; Sieffert, M.; Mullen, K.; Calderon, A.; Lazzaroni, R.; Bredas, J. L. *Chem.−Eur. J.* **2000**, *6* (20), 3739.
(33) Giancarlo, L. C.; Fang, H. B.; Rubin, S. M.; Bront, A. A.; Flynn, G. W. *J. Phys. Chem. B* **1998**, *102* (50), 10255.
(34) Miura, A.; Chen, Z. J.; Uji-i, H.; De Feyter, S.; Zdanowska, M.; Jonkheijm, P.; Schenning, A.; Meijer, E. W.; Wurthner, F.; De Schryver, F. C. *J. Am. Chem. Soc.* **2003**, *125* (49), 14968.
(35) Samori, P.; Severin, N.; Simpson, C. D.; Mullen, K.; Rabe, J. P. *J. Am. Chem. Soc.* **2002**, *124* (32), 9454.
(36) Samori, P.; Simpson, C. D.; Mullen, M.; Rabe, J. P. *Langmuir* **2002**, *18* (11), 4183.
(37) Samori, P.; Yin, X. M.; Tchebotareva, N.; Wang, Z. H.; Pakula, T.; Jackel, F.; Watson, M. D.; Venturini, A.; Mullen, K.; Rabe, J. P. *J. Am. Chem. Soc.* **2004**, *126* (11), 3567.
(38) Watson, M. D.; Jackel, F.; Severin, N.; Rabe, J. P.; Mullen, K. *J. Am. Chem. Soc.* **2004**, *126* (5), 1402.
(39) Yablon, D. G.; Giancarlo, L. C.; Flynn, G. W. *J. Phys. Chem. B* **2000**, *104* (32), 7627.
(40) Yablon, D. G.; Guo, J. S.; Knapp, D.; Fang, H. B.; Flynn, G. W. *J. Phys. Chem. B* **2001**, *105* (19), 4313.
(41) Yablon, D. G.; Wintgens, D.; Flynn, G. W. *J. Phys. Chem. B* **2002**, *106* (21), 5470.
(42) Walzer, K.; Sternberg, M.; Hietschold, M. *Surf. Sci.* **1998**, *415*, 376.
(43) Strohmaier, R.; Petersen, J.; Gompf, B.; Eisenmenger, W. *Surf. Sci.* **1998**, *418* (1), 91.
(44) Strohmaier, R.; Ludwig, C.; Petersen, J.; Gompf, B.; Eisenmenger, W. *Surf. Sci.* **1996**, *351* (1−3), 292.
(45) Müller, T.; Werblowsky, T. L.; Florio, G. M.; Berne, B. J.; Flynn, G. W., *Proc. Natl. Acad. Sci. U.S.A.*, in press.
(46) Ishikawa, Y.; Ohira, A.; Sakata, M.; Hirayama, C.; Kunitake, M. *Chem. Commun.* **2002**, (22), 2652.
(47) Griessl, S.; Lackinger, M.; Edelwirth, M.; Hietschold, M.; Heckl, W. M. *Single Molecules* **2002**, *3* (1), 25.
(48) Gopakumar, T. G.; Lackinger, M.; Hackert, M.; Muller, F.; Hietschold, M. *J. Phys. Chem. B* **2004**, *108* (23), 7839.
(49) Endo, O.; Toda, N.; Ozaki, H.; Mazaki, Y. *Surf. Sci.* **2003**, *545* (1−2), 41.
(50) Walzer, K.; Hietschold, M. *Surf. Sci.* **2001**, *471* (1−3), 1.
(51) Stecher, R.; Drewnick, F.; Gompf, B. *Langmuir* **1999**, *15* (19), 6490.
(52) Freund, J. E.; Edelwirth, M.; Krobel, P.; Heckl, W. M. *Phys. Rev. B* **1997**, *55* (8), 5394.
(53) Kemerink, M.; Offermans, P.; van Duren, J. K. J.; Koenraad, P. M.; Janssen, R. A. J.; Salemink, H. W. M.; Wolter, J. H. *Phys. Rev. Lett.* **2002**, *88* (9).
(54) Lei, S. B.; Wang, C.; Yin, S. X.; Wang, H. N.; Xi, F.; Liu, H. W.; Xu, B.; Wan, L. J.; Bai, C. L. *J. Phys. Chem. B* **2001**, *105* (44), 10838.
(55) Nowakowski, R.; Seidel, C.; Fuchs, H. *Phys. Rev. B* **2001**, *6319* (19).
(56) Scudiero, L.; Barlow, D. E.; Hipps, K. W. *J. Phys. Chem. B* **2000**, *104* (50), 11899.
(57) Frenklach, M. *Phys. Chem. Chem. Phys.* **2002**, *4*, 2028.
(58) Richter, H.; Howard, J. B. *Prog. Energy Combust. Sci.* **2000**, *26*, 565.
(59) Lindstedt, P.; Maurice, L.; Meyer, M. *Faraday Discuss.* **2001**, *119*, 409.
(60) Lu, M. M.; Mulholland, J. A. *Chemosphere* **2001**, *42* (5−7), 625.
(61) Mulholland, J. A.; Lu, M.; Kim, D. H. *Proc. Combust. Inst.* **2000**, *28*, 2593.
(62) Necula, A.; Scott, L. T. *J. Anal. Appl. Pyrolysis* **2000**, *54* (1−2), 65.
(63) Sonoda, M.; Itahashi, K.; Tobe, Y. *Tetrahedron Lett.* **2002**, *43* (30), 5269.
(64) Garcia, A. N.; Esperanza, M. M.; Font, R. *J. Anal. Appl. Pyrolysis* **2003**, *68−69*, 577.
(65) Fernandes, M. B.; Brooks, P. *Chemosphere* **2003**, *53* (5), 447.
(66) Wellmann, R.; Bottcher, A.; Kappes, M.; Kohl, U.; Niehus, H. *Surf. Sci.* **2003**, *542* (1−2), 81.
(67) *NIST Standard Reference Database*; National Institute of Standards and Technology: Washington, DC, 2003; No. 69.
(68) Gellman, A. J.; Paserba, K. R. *J. Phys. Chem. B* **2002**, *106* (51), 13231.
(69) Paserba, K. R.; Gellman, A. J. *J. Chem. Phys.* **2001**, *115* (14), 6737.
(70) Becke, A. D. *J. Chem. Phys.* **1993**, *98* (7), 5648.
(71) Lee, C. T.; Yang, W. T.; Parr, R. G. *Phys. Rev. B* **1988**, *37* (2), 785.
(72) Hay, P. J.; Wadt, W. R. *J. Chem. Phys.* **1985**, *82* (1), 270.
(73) *Jaguar*, version 4.1; Schrodinger Inc.: Portland, 2000.
(74) Stern, H. A.; Xu, H.; Harder, E.; Rittner, F.; Pavese, M.; Berne, B. J. *SIM Molecular Dynamics Program*.
(75) Schlick, T.; Fogelson, A. *J. Comput. Chem.* **1987**, *8* (7), 1025.

(76) Martyna, G. J.; Klein, M. L.; Tuckerman, M. *J. Chem. Phys.* **1992**, *97* (4), 2635.
(77) Steele, W. *Chem. Rev.* **1993**, *93* (7), 2355.
(78) Steele, W. A. *Langmuir* **1996**, *12* (1), 145.
(79) Bottani, E. J.; Bakaev, V.; Steele, W. *Chem. Eng. Sci.* **1994**, *49* (17), 2931.
(80) Jorgensen, W. L.; Tiradorives, J. *J. Am. Chem. Soc.* **1988**, *110* (6), 1666.
(81) From a low-density STM image of chrysene on graphite (1.85 V, 90 pA, 0.85% loop gain), the apparent height of the molecule is ∼60 pm. The apparent height of the graphite corrugation from the same image is ∼10 pm. From an STM image of bare graphite (1.90 V, 100 pA, 0.8% loop gain) without any background correction across a monatomic step, the step height is measured to be 230 pm. A second image of bare graphite, taken under identical conditions, gives a corrugation height for graphite of 15 pm. Assuming an expected step height for graphite of 3.35 Å, a corrected (scaled) molecular height of 1.31 Å is obtained for the height of a chrysene molecule lying flat on the graphite. This scaling, of course, is only approximate because the corrugation of graphite observed in STM images differs with tunneling conditions.
(82) The apparent molecular height from the high-density STM image was corrected using the scale factor generated by comparison of the low-density STM image of chrysene on graphite to that of bare graphite (see ref 81).
(83) Zacharias, D. E.; Prout, K.; Myers, C. B.; Glusker, J. P. *Acta Crystallogr.* **1991**, *B47*, 97.
(84) Krygowski, T. M.; Ciesielski, A.; Leszczynski, P. *Pol. J. Chem.* **1994**, *68*, 2097.
(85) Campbell, R. B.; Robertson, J. M.; Trotter, J. *Acta Crystallogr.* **1961**, *14*, 705.
(86) Jorgensen, W. L.; Severance, D. L. *J. Am. Chem. Soc.* **1990**, *112* (12), 4768.
(87) Hunter, C. A.; Sanders, J. K. M. *J. Am. Chem. Soc.* **1990**, *112*, 5525.
(88) Hill, T. L. *An Introduction to Statistical Thermodynamics*; Dover: New York, 1986.
(89) Deng, W. L.; Hipps, K. W. *J. Phys. Chem. B* **2003**, *107* (39), 10736.
(90) Scudiero, L.; Barlow, D. E.; Hipps, K. W. *J. Phys. Chem. B* **2002**, *106* (5), 996.
(91) Scudiero, L.; Barlow, D. E.; Mazur, U.; Hipps, K. W. *J. Am. Chem. Soc.* **2001**, *123* (17), 4073.
(92) Boschi, R.; Murrell, J. N.; Schmidt, W. *Faraday Discuss.* **1972**, *54*, 116.
(93) Adams, D. M.; Brus, L.; Chidsey, C. E. D.; Creager, S.; Creutz, C.; Kagan, C. R.; Kamat, P. V.; Lieberman, M.; Lindsay, S.; Marcus, R. A.; Metzger, R. M.; Michel-Beyerle, M. E.; Miller, J. R.; Newton, M. D.; Rolison, D. R.; Sankey, O.; Schanze, K. S.; Yardley, J.; Zhu, X. Y. *J. Phys. Chem. B* **2003**, *107* (28), 6668.
(94) Nitzan, A.; Ratner, M. A. *Science* **2003**, *300* (5624), 1384.
(95) Parker, V. D. *J. Am. Chem. Soc.* **1976**, *98* (1), 98.